Available online at www.sciencedirect.com
SCIENCE DIRECT®
Thermochimica Acta 430 (2005) 95–99
thermochimica acta
www.elsevier.com/locate/tca

Solidification of metallic tin in dispersed phase

Maria Grazia Bonicelli [a], Gianfranco Ceccaroni [b], Franco Gauzzi [c,*], Giuseppe Mariano [a]

[a] *Dipartimento ICMMPM, Università di Roma "La Sapienza", Sede di Chimica, Via del Castro Laurenziano 7, 00161 Rome, Italy*
[b] *Dipartimento di Scienze e Tecnologie Chimiche, Università di Roma "Tor Vergata", Via della Ricerca Scientifica, 00133 Rome, Italy*
[c] *Dipartimento di Ingegneria Meccanica, Università di Roma "Tor Vergata", Via del Politecnico 1, 00133 Rome, Italy*

Received 12 February 2004; received in revised form 2 December 2004; accepted 15 December 2004
Available online 5 February 2005

Abstract

Differential scanning calorimetry (DSC) and particle size measurements were carried out on disproportionation products of pure SnO to investigate the fusion and solidification behaviour of Sn droplets and their catalytic nucleation on Sn oxides. If disproportionation reaction takes place at $T \geq 798$ K, the products are metallic Sn and SnO_2; but for $523 < T < 798$ K, SnO_2 is replaced by an intermediate oxide (IO) $Sn_xO_{(1+x)}$. On melting, samples with IO show a drop of melting point of metallic tin due to Gibbs–Thomson effect; no lowering of melting point was observed in samples with SnO_2. On the other hand, if solidification occurs in the presence of IO, Tin droplets always displayed three distinct exothermic solidification peaks, but if it takes place in the presence of SnO_2, only one exothermic peak is observed. Undercooling values and contact angles were determined for each of the heterogeneous nucleation processes. The different behaviour of metallic Tin droplets was related to the different lattice symmetry of SnO_2 and IO, which act as nucleation catalysts.

Keywords: Heterogeneous nucleation; Solidification of tin; Nucleation catalysts; Tin oxides

1. Introduction

Heterogeneous nucleation and solidification behaviour of Sn droplets in a metal matrix were studied up by several authors. In particular Boswell and Chadwick [1] surveyed the nucleation rate of Sn-rich liquids in contact with solid Bi, Zn and Al; Kim and Cantor [2] examined the solidification of tin droplets embedded in an Al matrix and Park et al. [3] the solidification of tin droplets in an icosahedral Al–Cu–Fe quasi-crystalline matrix.

In all of these papers, the DSC solidification exotherms of Sn show two or more distinct [3] or partially overlapping peaks [1,2] with an undercooling ΔT of the order of 10^2 K.

The splitting of exothermal peaks was attributed to the solidification of Tin droplets on the boundaries and on different crystallographic planes of the matrix grains: e.g. $\{1\,0\,0\}_{Al}$ and $\{1\,1\,1\}_{Al}$ in the case of particles of tin embedded in an Al matrix. The contact angle ϑ for heterogeneous nucleation was also determined.

Another way of obtaining a fine dispersion of Sn particles is by the disproportionation reaction of SnO. One can get a powder that is an intimate mixture between Sn droplets and different Sn oxides as dispersing media according to the temperature and time of disproportionation.

This work deals with a DSC and particle size measurements on the disproportionation products of pure SnO with the aim of examining the fusion and solidification behaviour of Sn droplets and the catalytic nucleation on Sn oxides.

2. Materials and experimental

As reported in a previous work [4], Eq. (1) is the simplest representation of the monoxide disproportionation:

$$2SnO(s) = Sn(liq) + SnO_2(s) \quad (1)$$

* Corresponding author. Tel.: +39 06 72597184; fax: +39 06 2021351.
E-mail address: franco.gauzzi@uniroma2.it (F. Gauzzi).

0040-6031/$ – see front matter © 2004 Elsevier B.V. All rights reserved.
doi:10.1016/j.tca.2004.12.010

Table 1
Occurring phases and total Sn distribution (at.%) (from Ref. [4])

Sample	Phases	Sn(0)	Sn(II) in IO	Sn(IV) in IO	Sn(IV) in SnO_2
100 h/623 K	Sn, IO	17	58	25	
1 h/673 K	Sn, IO	17	59	24	
10 h/723 K	Sn, IO	18	60	22	
1 h/908 K	Sn, SnO_2	50			50

Nevertheless, for $523 < T < 798$ K, disproportionation gives an intermediate oxide (IO) whose composition is reported as Sn_3O_4 or Sn_2O_3, like the intermediate lead oxides. Therefore a more general reaction scheme should be adopted:

$$(1 + x)\,\mathrm{SnO} = \mathrm{Sn}_x\mathrm{O}_{1+x} + \mathrm{Sn} \quad (2)$$

where x is an integer ≥ 1.

No attempt to obtain the exact IO composition fully succeeded [5,6]. Nevertheless the IO is always monophasic and according to Ref. [7], has a triclinic lattice with constants $a = 5.457$ Å, $b = 8.173$ Å, $c = 3.714$ Å; $\alpha = 93.8°$, $\beta = 92.3°$, $\gamma = 90.0°$. This is also the IO structure in the samples used in our experiments.

The disproportionation products (in powder form) obtained at 100 h/623 K, 1 h/673 K, 10 h/723 K and 1 h/908 K, respectively, were selected for the present work. The presence of crystalline phases, along with the relative distribution of total Sn among Sn(0), Sn(II) and Sn(IV), is reported in Table 1.

The fusion and solidification behaviour of Sn in the samples was monitored with a Pyris 1 DSC device from Perkin-Elmer Instruments. Samples of about 30–35 mg were heated in graphite pans under N_2 atmosphere to prevent oxidation and then cooled. Heating and cooling took place at the rate of 2, 5, 10, 20 and 30 K/min.

For checking purposes, particle size measurements on some samples and SEM/EDS observation of sample disproportionated 1 h/673 K were also carried out.

3. Results

Figs. 1 and 2 show typical fusion and solidification DSC curves respectively, for each examined sample. It is worthwhile noting that, as far as fusion is concerned, only the sample 1 h/908 K shows a unique endothermic peak; other samples display two or more partially overlapping peaks. With regard to the solidification exotherm, we observe that – except once again the sample 1 h/908 K, showing a unique peak – each of the other three samples exhibits three well-separated peaks. Drop in melting point on fusion (ΔT_m) and undercooling on solidification (ΔT_s) are also easily observable.

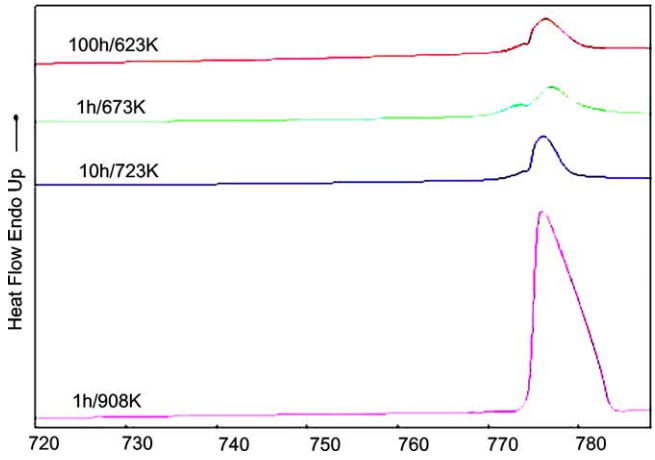

Fig. 1. Series of typical DSC melting curves of disproportionated SnO samples at 100 h/623 K; 1 h/673 K; 10 h/723 K; 1 h/908 K. Heating and cooling rate = 2 K/min for all curves.

4. Discussion

4.1. Melting of Sn droplets

First of all, let us consider the drop of melting point $\Delta T_m = T_m - T_0$ (T_0 = temperature at melting onset). It is well known that the melting point of spherical droplets of a pure metal depends on their radius r according to Gibbs–Thomson equation:

$$r = \frac{2\sigma}{\Delta G_v} \quad (3)$$

where σ is the surface tension of liquid, $\Delta\bar{G}_v = (L_v/T_m)\Delta T_m$ is the Gibbs free energy of fusion per unit volume, L_v the latent heat per unit volume and T_m the melting point of pure Tin. Then, the radius r as a function of ΔT_m

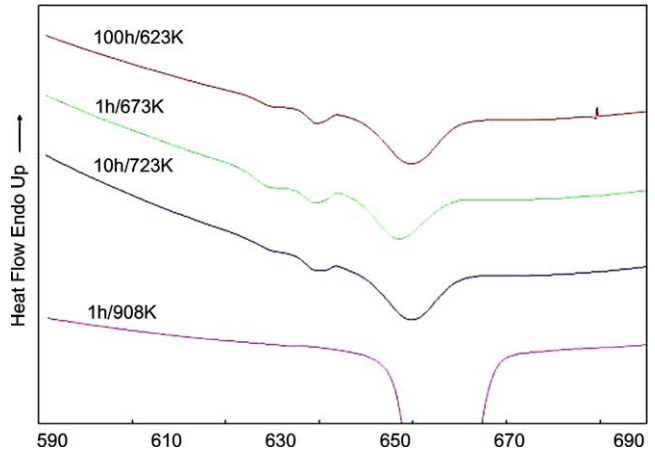

Fig. 2. Series of typical DSC solidification curves of disproportionated SnO samples at 100 h/623 K; 1 h/673 K; 10 h/723 K; 1 h/908 K. Heating and cooling rate = 2 K/min for all curves.

Table 2
Lowering of melting point of metallic tin and corresponding radius of spherical particles

Sample	ΔT_m (K)	r (μm) (calculated by Eq. (4))
100 h/623 K	3.33	0.38
1 h/673 K	4.58	0.28
10 h/723 K	3.11	0.41
1 h/908 K	0.50	2.52

can be written as follows:

$$r = \frac{2\sigma T_m}{L_v}\frac{1}{\Delta T_m} \tag{4}$$

Assuming for pure tin $\sigma = 550$ mN/m [8]; $T_m = 505$ K, $L_v = 4.4 \times 10^8$ J/m^3 [3], ΔT_m is easily appreciable from the thermograms. The observed results are reported in Table 2.

Considering, for example, the melting curve of the sample 1 h/673 K, Fig. 1 shows ($T_m \leq 4.58$ K; introducing these values, Eq. (4) gives $r \geq 0.29$ μm. Fig. 3 shows the cumulative distribution function of particle size in the same sample. Taking 0.2 K as a rough estimation of a minimum clearly detectable drop of melting point, this would correspond to a radius of ≅5 μm. According to the diagram in Fig. 3, the probability $P(r)$ of finding a particle with radius 0.3 μm $\leq r \leq$ 5 μm is $P \cong 40\%$. On the other hand Fig. 4 allows a direct observation of tin droplets in the SnO sample disproportionated at 1 h/673 K. Note that several tin droplets show a radius 0.3 μm $\leq r \leq$ 5 μm.

When disproportionation goes to SnO_2 (sample 1 h/908 K), the higher temperature and the different contact angle between Sn and dispersing phase (see below), allow an easier coalescence of liquid tin droplets and ΔT_m practically vanishes.

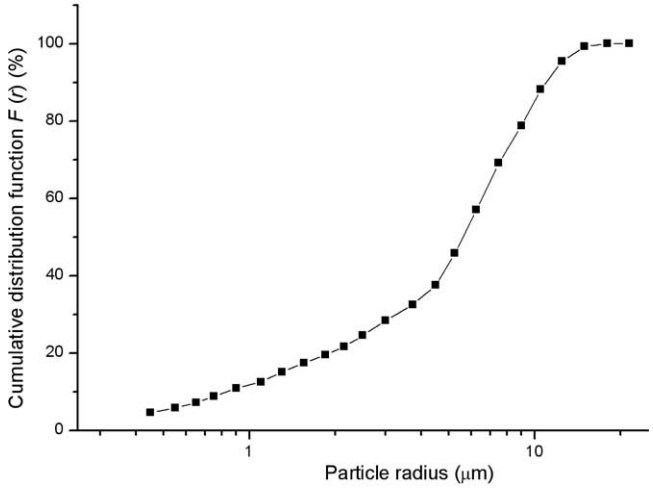

Fig. 3. Cumulative distribution function of particle radii in the sample 1 h/673 K.

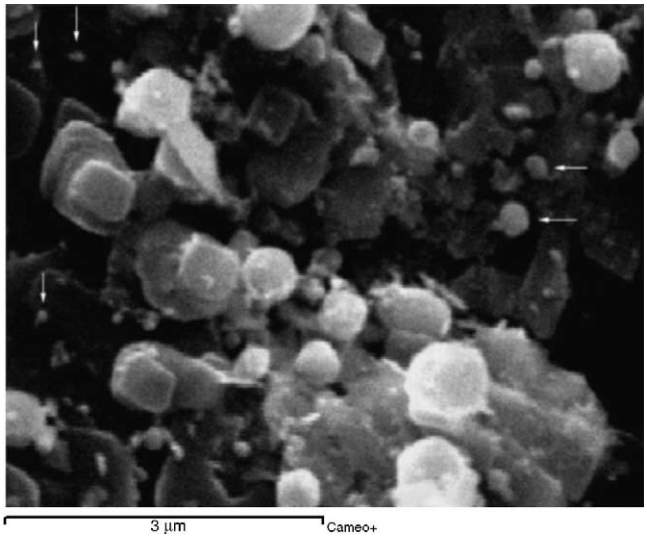

Fig. 4. SEM/EDS image of SnO disproportionation products (1 h/673 K). A number of spherical droplets that EDS analysis confirms to be constituted only by metallic Sn are visible. Arrows indicate the droplets which contribute by their radius to the lowering of melting point.

4.2. Solidification of Sn droplets

From classical theory of heterogeneous nucleation, the nucleation rate I within each droplet at a temperature $T < T_m$ is given by:

$$I = a \exp\left[\frac{-b}{(T_m - T)^2 T}\right] \tag{5}$$

where

$$a = n\frac{kT}{h}\exp\left(-\frac{\Delta G_\alpha}{kT}\right), \qquad b = \frac{16\pi}{3}\frac{\tau^3 T_m^2 f(\vartheta)}{L_v^2 k} \tag{6}$$

n is the number of possible nucleation sites per liquid droplet; k and h are Boltzmann's and Planck's constants, respectively; τ the solid/liquid interfacial energy (J m^{-2}); ΔG_α is the activation energy for transfer through solid–liquid interface; $f(\vartheta)$ is a function of contact angle ϑ given by $f(\vartheta) = (2 + \cos\vartheta)(1 - \cos\vartheta)^2/4$.Another fundamental equation states that the droplet solidification rate is given by the nucleation rate multiplied by the fraction of droplets still in liquid state:

$$\frac{dz}{dt} = I(1 - z) \tag{7}$$

where z is the fraction of solidified droplets.As pointed out in Refs. [2,3,9,10] by combining Eqs. (5) and (7) a relationship can be established between the peak temperature T_p of the exothermic solidification curve and the cooling rate R (K s^{-1}):

$$\ln\left(\frac{R(3T_p - T_m)}{(T_m - T_p)^3 T_p^2}\right) = \left[-\frac{b}{(T_m - T_p)^2 T_p}\right] + \ln\left(\frac{a}{b}\right) \tag{8}$$

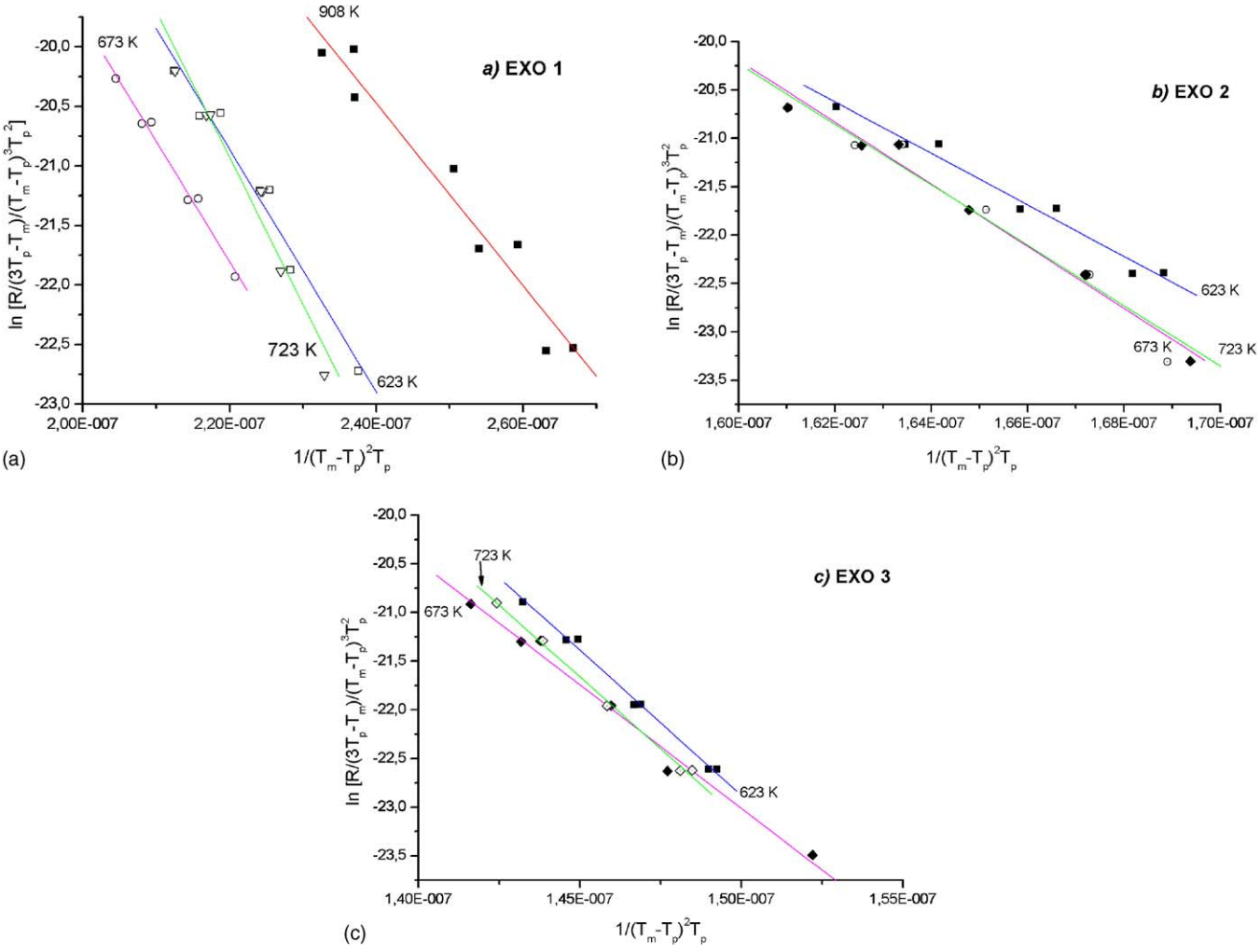

Fig. 5. Plots of $\ln[R(3T_p - T_m)/(T_m - T_p)^3 T_p^2]$ as a function of $1/(T_m - T_p)^2 T_p$ for (a) the first, (b) the second, and (c) the third exothermic solidification peak.

Eq. (8) shows a linear dependence of $\ln[R(3T_p - T_m)/(T_m - T_p)^3 T_p^2]$ on $1/(T_m - T_p)^2 T_p$, with slope = $-b$ and intercept = $\ln(a/b)$. Then, Eq. (6) allows to evaluate the contact angle ϑ and the number n of possible nucleation sites per liquid droplet. Notice that ϑ, the most significant parameter characterizing the particles of a nucleation catalyst, depends only on the slope of the straight lines of Eq. (8).

Fig. 5a shows the straight lines of Eq. (8) for the first solidification exothermic peak temperature of metallic Sn for all of the examined samples during cooling at 2, 5, 10, 20 and 30 K/min. Fig. 5b and c shows the straight lines with the same cooling rates for all samples except the 1 h/908 K one, that exhibits a unique solidification peak.

ϑ values were calculated using the slopes of the straight lines in Fig. 5 and collected in Table 3. In addition to the already mentioned values for T_m and L_v, $\tau = 84.4\ \mathrm{mJ\,m^{-2}}$ [3] and $\exp(-\Delta G/kT_m) \approx 10^{-2}$ [11] were also inserted into Eq. (6).

Experimental data clearly show that the nucleation and solidification behaviour of Sn strongly depends on the kind of Sn oxides, i.e. on the type of nucleation catalyst actually involved. If solidification takes place in the presence of SnO_2 (as in the disproportionated sample 1 h/908 K), only one solidification peak is observed; but if it occurs in the presence of IO (as in the remaining samples), we always have three distinct exothermic peaks. As shown by Fig. 5a, the straight line relative to the sample 1 h/908 K is quite apart from the lines pertaining to the other samples; moreover, the latter are almost coincident: the same observation holds for the exothermic peaks 2 and 3 characteristic of nucleation on IO (Fig. 5b and c). We think this is an indication that each peak

Table 3
Undercooling values and contact angles for each observed exothermic solidification peak

Sample	Exo 1		Exo 2		Exo 3	
	ΔT_s	ϑ	ΔT_s	ϑ	ΔT_s	ϑ
100 h/623 K	95.6	53	122.0	71	131.9	74
1 h/673 K	98.5	53	121.8	76	131.8	70
10 h/723 K	96.1	56	122.0	75	132.0	74
1 h/908 K	90.8	49	–	–	–	–

corresponds to the same type of nucleation events in the first three samples in Table 3 (see also the small differences in contact angles).

It is reasonable to ascribe this behaviour to the different crystallographic symmetry of the nucleation catalyst. In the case of SnO_2 (high-symmetry tetragonal lattice), the interfacial energy SnO_2/Sn seems to be practically independent of the crystallographic orientation of the SnO_2 plane on which nuclei are formed. This does not happen in the case of IO (low-symmetry triclinic lattice) where the three peaks should be assigned to Sn nucleation on planes with three different crystallographic orientations.

It is worth noting that in a study on the surface tension of liquid tin–oxygen alloys and its relationship with surface composition [12], a model based on the existence of oxide islands on the liquid Sn surface has been proposed. Islands are supposed to have a thickness of $\cong$0.5 nm and to be constituted by SnO, even though SnO_2 cannot be excluded, particularly in the zones that are richer in oxygen. Taking into account the structural features of the three different Tin oxides, the presence of such a film should make Sn nucleation easier on SnO_2 rather than on IO.

5. Conclusions

1. The main result is the different fusion and solidification behaviour displayed by Sn droplets when in the presence of either SnO_2 or IO.
2. As far as fusion is concerned, samples with IO show a lowering of melting point ΔT_m due to Gibbs–Thomson effect, while, in the presence of SnO_2 the higher temperature and the different values of contact angle between Sn and the dispersing phase allow an easier coalescence of liquid tin droplets so that r increases and ΔT_m practically vanishes.
3. If solidification occurs in the presence of IO we always have three distinct exothermic peaks, but if it occurs in the presence of SnO_2, only one exothermic peak is observed. The ϑ values, which have been determined for each peak, indicate a nucleation process quite different and an undercooling ΔT_s considerably lower in the presence of SnO_2. In the samples containing IO, on the other hand, each peak seems to correspond to the same nucleation process independently of the temperature and time of disproportionation. This behaviour is to be attributed to the different crystal symmetry of the nucleation catalyst. In the case of SnO_2, the crystallographic orientation of the plane on which nuclei are formed, does not seems to affect nucleation. In the case of IO, the three observed peaks should be ascribed to Sn nucleation on three crystallographic planes having different orientation.

Acknowledgments

The contributions of Dr. Patrizio Sbornicchia for the execution of particle size measurements and of Dr. Daniela Ferro (C.N.R.) for the SEM/EDS analysis are gratefully acknowledged.

References

[1] P.G. Boswell, G.A. Chadwick, Acta Metall. 28 (1978) 209.
[2] W.T. Kim, B.T. Cantor, J. Mater. Sci. 26 (1991) 2868.
[3] J.C. Park, W.T. Kim, D.H. Kim, J.R. Kim, Mater. Sci. Eng. A 304–306 (2001) 225.
[4] F. Gauzzi, B. Verdini, A. Maddalena, G. Principi, Inorg. Chim. Acta 104 (1985) 1.
[5] G.F. Ceccaroni, F. Gauzzi, S. Missori, Thermochim. Acta 165 (1990) 301.
[6] M.S. Moreno, et al., Solid State Ionics 144 (2001) 81.
[7] G. Murken, M. Trömel, Z. Anorg. Allgem. Chem. 397 (1973) 17.
[8] G. Lang, J. Inst. Met. 101 (1973) 300.
[9] W.T. Kim, D.L. Zhang, B. Cantor, Metall. Trans. A 22A (1991) 2487.
[10] B. Cantor, Keyna A.Q. O'Reilly, Curr. Opin. Solid State Mater. Sci. 2 (1997) 318.
[11] B. Cantor, R.D. Doherty, Acta Metall. 27 (1979) 33.
[12] R. Sangiorgi, C. Senillou, J.C. Joud, Surf. Sci. 202 (1988) 509.